

1 **Triple-element compound-specific stable isotope analysis (3D-CSIA): added**
2 **value of Cl isotope ratios to assess herbicide degradation**

3 Clara Torrentó^{1†*}, Violaine Ponsin^{1‡}, Christina Lihl², Thomas B. Hofstetter³, Nicole Baran⁴, Martin Elsner^{2,5},
4 Daniel Hunkeler¹

5 ¹Centre of Hydrogeology and Geothermics (CHYN), University of Neuchâtel, 2000 Neuchâtel, Switzerland

6 ²Helmholtz Zentrum München, Institute of Groundwater Ecology, 85764 Neuherberg, Germany

7 ³Eawag, Swiss Federal Institute of Aquatic Science and Technology, 8600 Dübendorf, Switzerland

8 ⁴BRGM, Bureau de Recherches Géologiques et Minières, 45060, Orléans CEDEX 02, France

9 ⁵Technical University of Munich, Chair of Analytical Chemistry and Water Chemistry, 81377 Munich, Germany

10 **Keywords:** Degradation, Isotope fractionation, Chlorine isotopes, Pesticides, Hydrolysis

11 **Synopsis:** This study demonstrates the benefit of including Cl isotope analysis for assessing pesticide in-
12 situ degradation

13 **Abstract**

14 Multi-element isotope fractionation studies to assess pollutant transformation are well-established for
15 point-source pollution, but are only emerging for diffuse pollution by micropollutants like pesticides.
16 Specifically, chlorine isotope fractionation is hardly explored but promising, because many pesticides
17 contain only few chlorine atoms so that “undiluted” position-specific Cl isotope effects can be expected
18 in compound-average data. This study explored combined Cl, N and C isotope fractionation to sensitively
19 detect biotic and abiotic transformation of the widespread herbicides and groundwater contaminants
20 acetochlor, metolachlor and atrazine. For chloroacetanilides, abiotic hydrolysis pathways studied under
21 acidic, neutral and alkaline conditions as well as biodegradation in two soils resulted in pronounced Cl
22 isotope fractionation (ϵ_{Cl} from -5.0 ± 2.3 to -6.5 ± 0.7 ‰). The characteristic dual C–Cl isotope fractionation
23 patterns ($\Lambda_{\text{C-Cl}}$ from 0.39 ± 0.15 to 0.67 ± 0.08) reveal that Cl isotope analysis provides a robust indicator of
24 chloroacetanilide degradation. For atrazine, distinct $\Lambda_{\text{C-Cl}}$ values were observed for abiotic hydrolysis
25 (7.4 ± 1.9) compared to previous reports for biotic hydrolysis and oxidative dealkylation (1.7 ± 0.9 and
26 0.6 ± 0.1 , respectively). The 3D isotope approach allowed differentiating transformations that would not
27 be distinguishable based on C and N isotope data alone. This first dataset on Cl isotope fractionation in
28 chloroacetanilides, together with new data in atrazine degradation, highlights the potential of using
29 compound-specific chlorine isotope analysis for studying in-situ pesticide degradation.

30 Introduction

31 Due to their extensive use in agriculture (4.1 M of tons applied worldwide in 2018)¹, pesticides are
32 increasingly detected in soils, surface water and groundwater, with the potential to affect ecosystems and
33 public health^{2, 3}. Despite numerous laboratory and field studies, it is still a major challenge to study
34 pesticide fate and degradation in aquatic and soil environments^{4, 5}. Current approaches rely on direct
35 measurements of parent compound concentrations, detection of transformation products, calculation of
36 metabolite-to-parent-compound ratios, or degradation gene abundance from molecular biology^{4, 6}.
37 Compound-Specific Isotope Analysis (CSIA) has increasingly been recognized as promising complementary
38 tool to provide evidence of transformation, and analytical methods are becoming available for pesticides⁷⁻
39 ⁹. During their transformation, contaminant molecules with light isotopes in the reactive position (*e.g.*,
40 ¹²C) are usually degraded at a different rate than those with heavy isotopes (*e.g.*, ¹³C). The resulting
41 isotope fractionation (*i.e.*, relative enrichment or depletion of molecules containing the heavier isotope
42 in the undegraded fraction) and the related kinetic isotope effects have the potential to provide
43 conclusive evidence of pesticide turnover, and unique insight into transformation mechanisms of
44 pesticides, independent of concentration trends.

45 Due to the complexity of their molecular structure, pesticides belong to different chemical families (*i.e.*,
46 with different functional groups) and are degraded by multiple (bio)chemical reaction pathways⁴. For
47 most of these pathways, the extent of isotope fractionation is unknown. In addition, the extent of intrinsic
48 isotope fractionation associated with specific (bio)chemical transformations can be modified by steps that
49 do not cause isotope fractionation, but that are partially rate-determining such as mass transfer processes
50 in the microbial cell^{10,11}. In this case, the measured isotope fractionation may not reflect the actual isotope
51 fractionation induced by the (enzymatic) reaction. Since this effect typically affects both elements in the
52 reaction bond(s), the monitoring of isotope values for two or three elements (2D-CSIA or 3D-CSIA) offer
53 more reliable identification and quantification of the transformation process(es) involved than single-
54 element CSIA. The added benefit of a multi-element approach has already been demonstrated for point-
55 source pollution by legacy compounds^{12,13, 14}, but is only emerging for diffuse pollution by organic

56 micropollutants such as pesticides. As most pesticides contain many carbon atoms, changes in carbon
57 isotope ratios at the reactive site may be considerably diluted by non-reacting carbon atoms at other
58 positions, for which isotope values do not change^{7, 15}. As pesticides typically contain only one or few
59 heteroatoms (such as N, S, O or Cl), isotope ratios of these elements are particularly interesting since
60 measured isotope fractionation for these elements is not expected to be affected by “dilution effects”.
61 Several studies have already assessed dual (C and N, or C and H) or even triple (C, N and H) isotope
62 fractionation during pesticide transformation processes^{10, 11, 16-26}, but halogen isotopes have not yet been
63 included.

64 Here, chlorine is a particular promising element also because many transformation pathways involve
65 breaking of C–Cl bonds during the initial step of degradation^{21, 27-29}. A larger isotope fractionation in the
66 compound-average is thus expected for chlorine than for carbon^{7, 15}. We recently developed a routine and
67 cost-efficient method to measure Cl isotope ratios with a widely available gas chromatograph (GC)-single
68 quadrupole mass spectrometer (qMS) in three model herbicides frequently detected in water resources:
69 the triazine atrazine (ATR) and the chloroacetanilides acetochlor (ACETO) and metolachlor (METO)³⁰. This
70 Cl-CSIA method, in combination with existing methods for C- and N-CSIA⁸, has the potential to provide
71 new insights into transformation processes of these compounds²⁸. To further corroborate the benefit of
72 a 3D-CSIA approach including chlorine isotope data, multiple research gaps warrant investigation. For
73 example, with carbon and nitrogen isotope data only, it is currently not possible to distinguish ATR
74 oxidative dealkylation from alkaline hydrolysis or acidic hydrolysis from biotic hydrolytic dechlorination.
75 For chloroacetanilides degradation, multi-element isotope studies including chlorine isotope data are
76 even missing completely.

77 Biodegradation is especially relevant for the transformation of chloroacetanilides in the environment but
78 most pathways for microbial transformation are unknown³¹, and the associated isotope data are missing.
79 The most common chloroacetanilide degradation pathway is enzyme-catalyzed thiolytic dechlorination to
80 the ionic ethane sulfonic acid (ESA) and oxanilic acid (OXA) metabolites, which are frequently detected in

81 ground and surface water³²⁻³⁵. The first step of this reaction is an S_N2 nucleophilic substitution at the
82 chlorinated carbon by glutathione as nucleophile^{36, 37}. Abiotic chloroacetanilide dechlorination to ESA
83 metabolites can also be important under sulfate-reducing conditions by reaction with reduced sulfur
84 nucleophiles³⁸⁻⁴¹. Despite its importance, only few studies have assessed C and N isotope fractionation
85 during biologically-catalyzed thiolytic dechlorination of ACETO and METO⁴²⁻⁴⁵. Although hydrolytic
86 dechlorination of chloroacetanilides (*i.e.*, S_N2 nucleophilic substitution of chloride by OH or H₂O) is
87 expected to be limited at the circumneutral pH encountered in soil and water, significant production of
88 the hydroxylated degradation products has been reported in soil extracts^{46, 47}, surface water⁴⁸,
89 groundwater³³ and surface and subsurface drinking water sources³². Masbou et al.²¹ reported the only
90 available dataset on C and N isotope fractionation during abiotic hydrolysis of ACETO and METO. For
91 ACETO, C isotope fractionation has been reported for biodegradation in lab-scale wetlands under anoxic
92 conditions, for which the degradation mechanism is unknown⁴⁹. For other chloroacetanilide
93 transformations (such as N-dealkylation or O-demethylation), isotope fractionation has not been assessed
94 yet.

95 Hydrolytic dechlorination is also a common natural attenuation process for ATR⁵⁰⁻⁵³, which is expected to
96 occur by acid-catalyzed hydrolysis mediated by bacteria and fungi²². Abiotic ATR hydrolysis may also occur
97 at high or low pH, and by abiotic mineral-catalyzed reactions⁵⁴. Desethylatrazine and desisopropylatrazine
98 are among the main ATR metabolites found in groundwater, formed mainly through a biotic oxidative N-
99 dealkylation pathway⁵¹⁻⁵³. Whereas C and N isotope fractionation during these ATR degradation processes
100 has been previously reported^{10, 11, 21-26, 55, 56}, our recent 3D-CSIA study was the first to include Cl isotope
101 data for ATR degradation and to allow distinguishing ATR biodegradation by oxidative dealkylation and
102 hydrolytic dechlorination²⁸. It is therefore unknown yet whether Cl isotopes could help to distinguish
103 between other processes relevant for the transformation of ATR in an environmental context, such as
104 biotic hydrolytic dechlorination from abiotic hydrolysis – pathways that are indistinguishable on a dual
105 C/N isotope basis^{22, 23}.

106 The goal of this study was thus to assess whether Cl is a sensitive indicator for different transformations
107 of these three model herbicides (ACETO, METO, ATR) and whether the additional information gained from
108 Cl isotope fractionation can help in distinguishing different transformation pathways. The specific
109 objectives were (1) to determine Cl, C and N isotope fractionation and dual-isotope slopes during abiotic
110 hydrolysis of ACETO, METO and ATR under acidic, alkaline and neutral conditions and during METO
111 biodegradation in two agricultural soils; (2) to gain mechanistic insights for these transformation
112 reactions; and (3) to provide 2D- and 3D-element isotope fractionation patterns that can distinguish
113 degradation pathways of these three environmentally relevant pesticides in future field studies. Abiotic
114 experiments allow characterizing specific degradation mechanisms and provide reference multi-isotopic
115 fractionation values, which are critical for assessing the feasibility of CSIA for distinguishing degradation
116 pathways and evaluating pesticide transformations in the field.

117 **Materials and Methods**

118 - **Hydrolysis experiments**

119 A list of chemicals and detailed experimental descriptions are available in the **Supporting Information**
120 **(SI)**. Triplicate experiments were performed in the dark for each experimental condition (acidic, neutral
121 and alkaline) in 250 mL serum flasks. Buffer solutions were prepared at pH 3, 7 and 12 and spiked with 50
122 mg/L ACETO, METO or ATR from 2 g/L (ACETO and METO) or 1 g/L (ATR) stock solutions in MeOH:water
123 (50:50 v:v). The final MeOH content was 2.5% v:v for ATR, and 1.5% for ACETO and METO experiments.
124 This high initial concentration was chosen for ease of the isotopic measurements, as it is not expected to
125 have any influence on isotope fractionation. Nevertheless, CSIA at lower environmentally relevant
126 concentrations is also feasible using extensive sample preparation procedures^{8,30}. The flasks were capped
127 with screw caps and incubated at 60±1°C (ACETO and METO at pH 12 and 7), 80±1°C (ACETO and METO
128 at pH 3 and 7), and 25±1°C (ATR experiments). These temperatures were chosen to obtain reactant
129 turnover within manageable time scales based on previously reported activation energies and second-
130 order rate constants^{21,27,57}. The temperature dependence of isotope fractionation is small and within the
131 limits of uncertainty (see below). The pH value of the solutions was monitored over time and eleven-

132 milliliter aliquots were sampled at regular intervals for concentration and isotope analysis. The reaction
133 was stopped with 20 μL of a 40% HNO_3 solution (alkaline hydrolysis) or 65 μL of a 24 M NaOH solution
134 (acidic hydrolysis) to obtain a circumneutral pH. Toward the end of the reaction, larger aliquot volumes
135 (26, 36 or 41 mL) were sampled to collect sufficient mass for concentration and isotope analyses. Volumes
136 of HNO_3 and NaOH were adjusted accordingly. Once the reaction was stopped, all vials including those for
137 experiments at pH 7 were kept at 4°C until processing.

138 Five to ten milliliters (up to 38 mL for selected samples toward the end of the reaction) of the aliquots
139 were extracted by SPE as explained elsewhere³⁰. Eluates were evaporated until dryness followed by
140 reconstitution with appropriate volumes of EtAc for GC-qMS and GC-IRMS injections. The whole SPE-CSIA
141 method was previously validated^{8,30}, and was shown to have negligible isotope effects ($\Delta\delta^{37}\text{Cl} \leq 1\text{‰}$, $\Delta\delta^{13}\text{C}$
142 $\leq 0.5\text{‰}$ and $\Delta\delta^{15}\text{N} \leq 1\text{‰}$). The remaining volume of each aliquot was used for determining analyte
143 concentrations.

144 - **Soil degradation experiments**

145 Two agricultural soils (soil M and soil V) were used. Details about the two soils are shown in **Table S2**. The
146 ponderal water content was determined and adjusted to 15 g/100 g soil with sterilized water, a value
147 close to the assumed 80% of the water holding capacity. 50 g of each soil were placed in glass pots and
148 spiked with METO to achieve a final concentration of approximately 2.5 mg/kg. After the spiking, each
149 glass pot was placed into a larger glass jar containing a 10 mL flask of deionized water to maintain a
150 constant humidity during the experiment. The jars were tightly sealed and incubated in the dark in a
151 thermostated chamber (25°C). Experiments were performed in triplicate. Soils without spiking were
152 incubated in the same conditions to confirm the absence of METO in the soil before spiking and that no
153 METO is released with time.

154 Soil samples were extracted using a QuEChERS[®] extraction kit. Briefly, 5 g of soil were placed in a 50 mL
155 tube and 80 μL of a surrogate (5 mg/L metolachlor-d6 in acetonitrile, an amount 20-70 times smaller than
156 the non-labelled compound, see the **SI** for details), 8 mL of 30 mM KH_2PO_4 and 10 mL of 5% formic acid in

157 acetonitrile were added. The tube was shaken manually during 30 seconds and the extraction salts (4 g
158 MgSO₄, 1 g NaCl, 1 g sodium citrate, 0.5 g disodium citrate sesquihydrate) were added. The mixture was
159 agitated during 1 min and centrifuged (4000 rpm) during 5 minutes. The supernatant was transferred to
160 another tube and the extract volume was adjusted to 2 mL with acetonitrile. Extractions were performed
161 in triplicates and the three resulting extracts were combined in one. Details about additional extraction
162 tests performed for assessing Cl and C isotope fractionation during soil extraction can be found in the **SI**.
163 The extraction was shown to induce a systematic but reproducible isotope fractionation for Cl ($\Delta\delta^{37}\text{Cl}$
164 between +2.5 and +3.5‰) and no fractionation for C. There was no significant effect of the deuterated
165 compound used as a surrogate on the determination of the C isotope ratios, as discussed in the **SI**.

166 - **Analytical methods**

167 Detailed descriptions of analytical methods are available in the **SI**. Briefly, for hydrolysis experiments,
168 concentrations of parent compounds (ACETO, METO and ATR) and hydroxylated transformation products
169 (2-hydroxy-acetochlor – HACETO, 2-hydroxy-metolachlor – HMETO, and 2-hydroxy-atrazine – HATR) were
170 determined by ultra-high pressure liquid chromatography quadrupole time of flight mass spectrometry
171 (UHPLC-QTOF-MS) following a method described elsewhere⁸. Other transformation products were
172 tentatively identified, based on the exact molecular weight and fragmentation patterns. METO and
173 metabolite concentrations in the soil extracts were determined by ultra-performance liquid
174 chromatography–triple quadrupole mass spectrometry (UPLC-QqQ-MS) as detailed in the **SI**. Cl isotope
175 ratios were measured by GC-qMS following the method by Ponsin et al.³⁰, using the two-point calibration
176 approach and applying corrections to take into account fragments with two ¹³C atoms. C and N isotope
177 ratios in the extracts were measured by GC-IRMS, as explained elsewhere⁸.

178 Calculation of chlorine, carbon and nitrogen isotope ratios

179 Cl, C and N isotope values are reported in per mil (‰) using the delta notation (δ) relative to the
180 international reference points Mean Ocean Chloride (SMOC), Vienna PeeDee Belemnite (V-PDB) and air,
181 respectively:

182
$$\delta E(\text{in } \text{‰}) = \left(\frac{R_E}{R_{E,\text{std}}} - 1 \right) \quad (1)$$

183 where E is the considered element (Cl, C or N), R_E and $R_{E,\text{std}}$ are the isotope ratios of the element E in the
 184 sample and the corresponding reference compound, respectively. Reported isotope ratios are expressed
 185 as arithmetic means of replicate measurements with uncertainties of $\pm 0.5\text{‰}$ for C and $\pm 1.0\text{‰}$ for Cl and
 186 N (related to the extraction method), except when higher standard deviation ($\pm 1\sigma$) in $\delta^{13}\text{C}$ and $\delta^{15}\text{N}$ values
 187 or higher total uncertainty for $\delta^{37}\text{Cl}$ was found. For $\delta^{37}\text{Cl}$ measurements, total uncertainty was calculated
 188 taking into account uncertainties (as standard error of the mean) associated with sample measurement
 189 and with the measurement of the two standards as explained elsewhere³⁰. The reference values for the
 190 in-house isotope standards used in this study are provided in **Table S1**.

191 - **Evaluation of stable isotope data**

192 Isotope fractionation (ϵ) values for chlorine, carbon and nitrogen were obtained from the slope of the
 193 linearized Rayleigh equation:

194
$$\ln \left(\frac{\delta E_t + 1}{\delta E_0 + 1} \right) = \epsilon_E \times \ln f \quad (2)$$

195 where δE_0 and δE_t are isotope values of element E in the beginning (0) and at any given time (t),
 196 respectively, and f is the fraction of substrate remaining at time t . Errors given for ϵ values correspond to
 197 the 95% Confidence Interval (CI) of the linear regression in Rayleigh plots.

198 To determine the intrinsic isotope effect of the bond cleavage, the position-specific apparent kinetic
 199 isotope effects (AKIEs) were calculated according to the following equation⁵⁸:

200
$$AKIE_E \approx \frac{1}{1 + \frac{z \times n}{x} \times \epsilon_{E,\text{bulk}}} \quad (3)$$

201 where n is the number of atoms of the considered element, x is the number of these atoms located at the
 202 reactive site/s, z is the number of atoms located at the reactive site/s and being in intramolecular
 203 competition. The values for n , x , and z were chosen depending on the considered reaction mechanism.

204 Details about the parameters chosen for AKIE calculations are explained in the **SI (Table S5)**. The
205 uncertainty of AKIE values was estimated by error propagation.

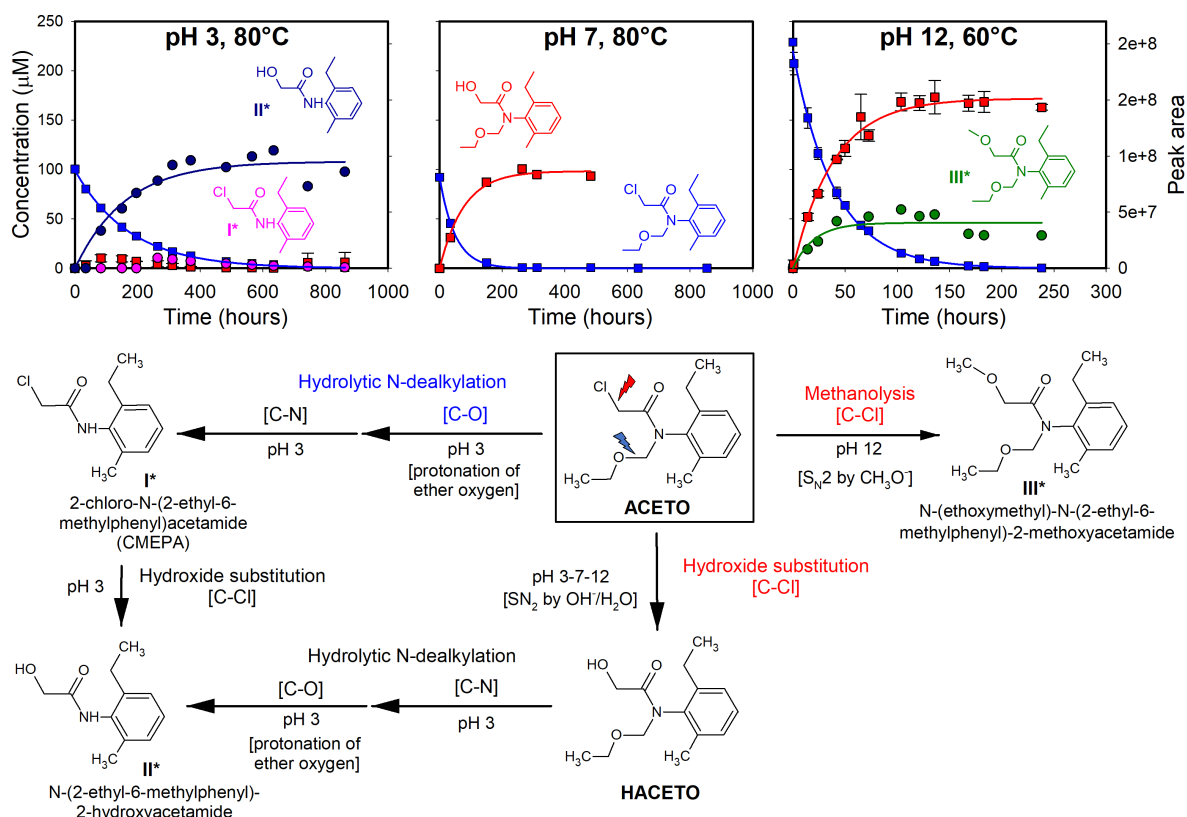
206 Dual-element isotope fractionation patterns for different degradation pathways were characterized by
207 the slope of the Ordinary Linear Regressions (OLR) in a 2D-isotope plot, *i.e.*, $\Lambda_{C/Cl} = \Delta\delta^{13}C/\Delta\delta^{37}Cl$, $\Lambda_{N/C} =$
208 $\Delta\delta^{15}N/\Delta\delta^{13}C$ and $\Lambda_{N/Cl} = \Delta\delta^{15}N/\Delta\delta^{37}Cl$. The uncertainty of $\Delta\delta$ values was estimated by error propagation.
209 For reporting the uncertainty of Λ , the 95% CI and the standard error (SE) of the slope are shown. The
210 York regression method, proposed by Ojeda et al.⁵⁹ to incorporate measurement error in both the x- and
211 y-variables in 2D isotope plots, was also assessed.

212 Statistical differences between the different experimental conditions and with previously reported values
213 for the estimated isotope fractionation values (ϵ_{Cl} , ϵ_C and ϵ_N) and 2D-isotope slopes (Λ_{C-Cl} , Λ_{N-C} and Λ_{N-Cl})
214 were assessed using statistical two-tailed z-score tests⁵⁹. Differences were considered statistically
215 significant at the $\alpha = 0.05$ confidence level.

216 **Results and Discussion**

217 **Transformation Pathways and Associated Isotope Effects in Abiotic Acetochlor Hydrolysis**

218 ACETO transformation followed pseudo first-order kinetics, with half-lives ranging between 1.1 and 5.4
219 days (**Table S8**). At pH 7, ACETO degradation was observed at 80°C, whereas it was not significantly
220 degraded at 60°C (**Fig. S3**). **Figure 1** shows the time courses for the disappearance of ACETO and the
221 appearance of its transformation products.



222
 223 **Figure 1.** Time courses and postulated possible degradation pathways for acidic (80°C), neutral (80°C),
 224 and alkaline (60°C) hydrolysis of ACETO. Concentration of ACETO (blue squares) and the hydroxylated
 225 product HACETO (red squares) is shown for triplicate experiments. Error bars stand for the standard
 226 deviation of concentrations in triplicate experiments. The peak areas obtained by UHPLC-QTOF-MS are
 227 shown for the non-hydroxylated transformation **products I** (pink circles), **II** (dark blue circles) and **III** (green
 228 circles). Solid lines represent model fits assuming pseudo-first-order transformation. * denotes a putative
 229 structure. The details about the tentatively identified transformation products are shown in **Figure S4**.

230 At pH 7, a unique hydroxylated degradation product, HACETO, was produced. It is therefore expected that
 231 the whole reaction involved exclusively cleavage of the C–Cl bond as the first rate-limiting step through a
 232 S_N2 nucleophilic substitution mechanism. Accordingly, the reaction resulted in a significant normal isotope
 233 effect for both chlorine ($\epsilon_{\text{Cl}} = -5.7 \pm 1.2\%$) and carbon ($\delta^{13}\text{C}$ shift of +11‰ after 150 days, although ϵ_{C} could
 234 not be estimated because the linear regression is not statistically significant, $p > 0.05$) (**Table 1**). The
 235 obtained AKIE_{Cl} value (1.006, **Table S9**) is consistent with the expected range of primary chlorine isotope
 236 effects in an S_N2 type reaction (AKIE_{Cl} = 1.006 - 1.009^{60, 61}). As consequence of exclusive C–Cl bond
 237 cleavage, N isotope fractionation was negligible (**Fig. S5**).

238 **Table 1.** Carbon, nitrogen and chlorine isotope fractionations (ϵ_C , ϵ_N , ϵ_{Cl}) and 2D-isotope slopes ($\Lambda_{N/C}$, $\Lambda_{C/Cl}$
 239 and $\Lambda_{N/Cl}$) for acidic, neutral and alkaline hydrolysis of ACETO, METO and ATR and for METO degradation
 240 in soil. ϵ and Λ values were calculated by OLR and uncertainty is shown as the 95% confidence interval
 241 (95% CI). When differences between the results obtained at different experimental conditions were not
 242 significant ($p>0.05$), data were merged to derive combined ϵ and Λ values. n.s = not significant; n.a = not
 243 analyzed.

| | ϵ_C (‰) ± 95% CI | ϵ_N (‰) ± 95% CI | ϵ_{Cl} (‰) ± 95% CI | $\Lambda_{N/C}$ ± 95% CI | $\Lambda_{C/Cl}$ ± 95% CI | $\Lambda_{N/Cl}$ ± 95% CI |
|-------------------------------------|------------------------------|------------------------------|---------------------------------|-----------------------------|------------------------------|------------------------------|
| Acetochlor hydrolysis | | | | | | |
| pH 3 (80°C) | -3.2±0.3 | n.s | -4.2±0.5 | n.s | 0.72±0.08 | n.s |
| pH 7 (80°C) | n.s | n.s | -5.7±1.2 | n.s | n.s | n.s |
| pH 12 (60°C) | -4.0±1.2 | n.s | -5.3±0.4 | n.s | 0.65±0.24 | n.s |
| Combined data (pH3&pH12&pH7) | -3.5±0.5 | n.s | -5.1±0.5 | n.s | 0.67±0.08 | n.s |
| Metolachlor hydrolysis | | | | | | |
| pH 3 (80°C) | -4.7±0.7 | n.s | -9.0±3.1 | n.s | 0.51±0.20 | -0.32±0.28 |
| pH 7 (60°C) | -3.8±1.1 | n.s | -12.1±7.1 | n.s | n.s | n.s |
| pH 7 (80°C) | -4.0±0.8 | n.s | -6.4±1.4 | n.s | 0.87±0.16 | n.s |
| pH 12 (60°C) | -3.9±1.3 | n.s | -6.8±1.5 | n.s | 0.55±0.13 | n.s |
| Combined data (pH3&pH12&pH7) | -4.1±0.4 | n.s | -6.5±0.7 | - | 0.55±0.09 | - |
| Metolachlor soil degradation | | | | | | |
| Soil M | -2.0±1.2 | n.a | -3.3±2.4 | n.a | 0.51±0.28 | n.a |
| Soil V | -2.6±1.3 | n.a | -3.6±2.4 | n.a | n.s. | n.a |
| Combined data (soilM&soilV) | -2.4±0.8 | n.a | -3.3±1.6 | n.a | 0.53±0.22 | n.a |
| Atrazine hydrolysis | | | | | | |
| pH 3 (25°C) | -4.7±0.3 | 2.7±0.4 | -0.54±0.11 | -0.61±0.08 | 8.3±1.5 | -4.8±1.7 |
| pH 12 (25°C) | -4.0±3.3 | -1.3±1.1 | -0.59±0.22 | 0.32±0.17 | n.s | n.s |
| Combined data (pH3&pH12) | -4.5±0.6 | - | -0.60±0.13 | - | 7.4±1.9 | - |

244

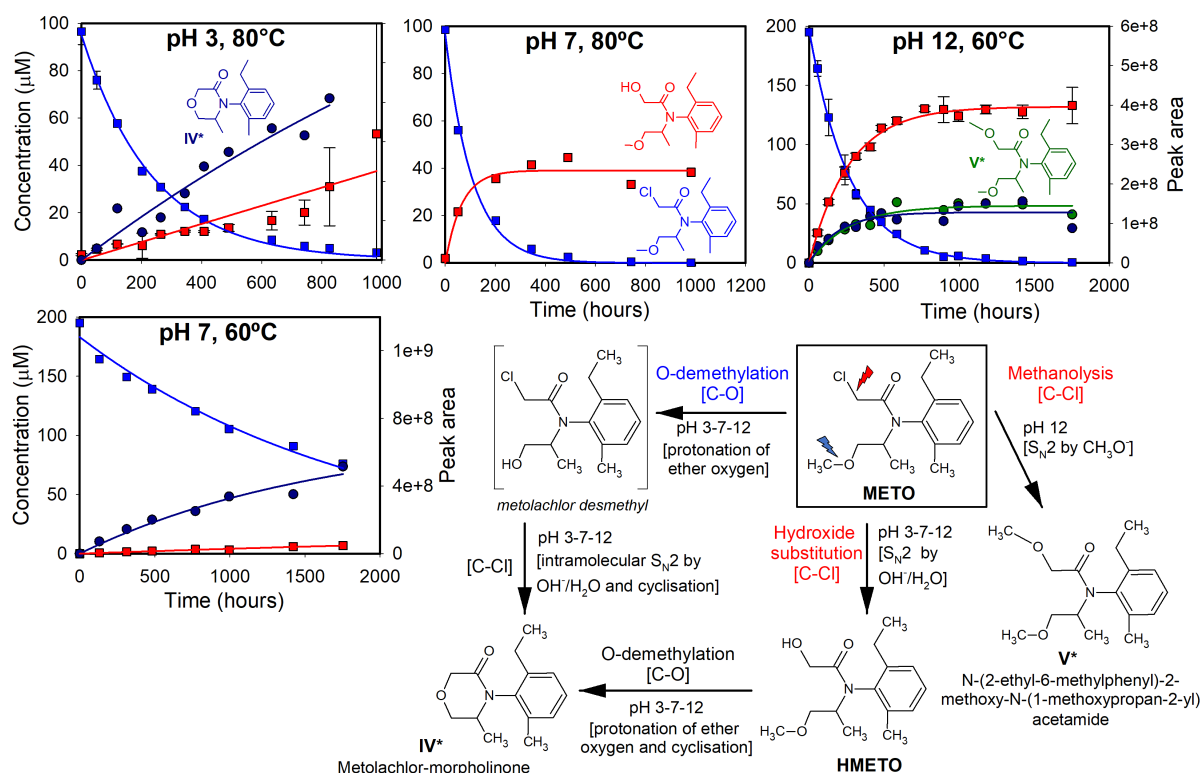
245 At pH 12 (60°C), the hydroxylated product HACETO accounted for about 65% of ACETO degradation (**Fig.**
 246 **1**), pointing again to nucleophilic hydrolysis of the C–Cl bond as the main degradation pathway, as
 247 observed by previous studies^{21, 27}. In our experiments, however, a different transformation product was
 248 also detected (product III), pointing to an additional degradation pathway. The spectrum of product III
 249 suggests that it is a methanolysis product of ACETO, where Cl⁻ was replaced by H₃CO⁻ (**Fig. S4**). It was
 250 tentatively identified as N-(2,6-Diethylphenyl)-N-(ethoxymethyl)-2-hydroxyacetamide, which might have
 251 been formed as a by-product of the hydrolysis experiment in the presence of methanol under alkaline
 252 conditions by nucleophilic substitution of the chlorine atom by CH₃O⁻⁶². The chlorine isotope effect at pH
 253 12 (ϵ_{Cl} = -5.3±0.4‰) was indistinguishable to that found under neutral conditions (ϵ_{Cl} = -5.7±1.2‰),

254 confirming that both cases involved initial cleavage of the C–Cl bond via a S_N2 nucleophilic substitution
255 mechanism. A ϵ_C value of $-4.0\pm 1.2\%$ was obtained, which is not significantly different from the value
256 reported by Masbou et al.²¹ for alkaline hydrolysis of ACETO at 20–30°C ($-4.0\pm 0.8\%$, **Table S9**), where
257 HACETO was the only product. Obtained $AKIE_{Cl}$ (1.005 ± 0.0004) and $AKIE_C$ (1.059 ± 0.019) values are
258 consistent with the typical ranges of primary carbon and chlorine isotope effects for S_N2 type mechanisms
259 ($AKIE_{Cl} = 1.006 - 1.009$ ^{60, 61} and $AKIE_C = 1.03 - 1.09$ ⁵⁸). Like at pH 7, insignificant N isotope fractionation was
260 observed, consistent with previous experiments at 20–30°C²¹.

261 At pH 3 (80°C), HACETO accounted for only 10% of ACETO degradation (**Fig. 1**) indicating either further
262 degradation of HACETO, or that an additional pathway may have played a significant role. Two additional
263 transformation products were detected, referred to as products **I** and **II**. Product **I**, which contains one Cl
264 atom, was tentatively identified as the N-dealkylated product 2-Chloro-N-(2-ethyl-6-
265 methylphenyl)acetamide (CMEPA). Hydrolytic N-dealkylation of ACETO to CMEPA was previously
266 observed²⁷ under strong acidic conditions ($pH \leq 1$). This reaction involves an initial protonation of the ether
267 C–O bond followed by a transient imine formation, rather than an initial cleavage of the C–Cl bond.
268 Therefore, a chlorine isotope effect is not expected. Product **II**, which does not contain any Cl atom, was
269 tentatively identified as N-(2-ethyl-6-methylphenyl)-2-hydroxyacetamide. This product might have
270 formed by two different pathways: (1) hydrolysis (*i.e.*, S_N2 nucleophilic hydroxide substitution) of the
271 amide linkage in product **I** (CMEPA), as suggested by Carlson et al.²⁷ for strong acidic conditions, and (2)
272 nucleophilic substitution at the ether C–O bond of HACETO. Substantial amounts of product **II** appeared
273 before the appearance of product **I** (**Fig. 1**), pointing to the involvement of HACETO as intermediate.
274 Although further research is required, the observation of still pronounced but smaller chlorine isotope
275 fractionation ($\epsilon_{Cl} = -4.2\pm 0.5\%$) suggests indeed that HACETO was involved as intermediate in product **II**
276 formation, but that the hydrolytic dealkylation pathway involving product **I** as intermediate also played a
277 significant role. Insignificant N isotope fractionation was observed, consistent with the proposed
278 pathways, in which C–N bonds cleavage is not involved as initial reaction step.

279 **Transformation Pathways and Associated Isotope Effects in Abiotic Metolachlor Hydrolysis**

280 METO degradation was observed under pH 3 (80°C), pH 12 (60°C) and pH 7 (80°C and even 60°C, **Fig. 2**),
 281 with half-lives ranging between 4.2 and 58 days (**Table S8**). Two main transformation products were
 282 detected (**Fig. 2**): the hydroxylated product HMETO, which has been previously reported mainly under
 283 alkaline conditions^{21, 27}, and product **IV**, tentatively identified as 4-(2-Ethyl-6-methylphenyl)-5-methyl-3-
 284 morpholinone (metolachlor-morpholinone). This morpholinone derivative has already been detected for
 285 METO degradation under strongly acidic conditions and in long-term near-neutral pH experiments at
 286 room temperature²⁷.



287 **Figure 2.** Time courses and postulated possible degradation pathways for acidic (80°C), neutral (at 60 °C
 288 and 80 °C) and alkaline (60°C) hydrolysis of METO. Concentration of METO (blue squares) and the
 289 hydroxylated product HMETO (red squares) is shown for triplicate experiments. Error bars stand for the
 290 standard deviation of concentrations in triplicate experiments. The peak areas obtained by UHPLC-QTOF-
 291 MS are shown for the non-hydroxylated transformation **products IV** (dark blue circles), and **V** (green
 292 circles). Solid lines represent model fits assuming pseudo-first-order transformation. * denotes a putative
 293 structure. The structure in brackets indicates a postulated intermediate, not detected in the present
 294 experiments. The details about the tentatively identified transformation products are shown in **Figure S4**.
 295

296 Under both neutral and acidic conditions, both HMETO (which accounted for about 50-55% of the METO
297 degradation) and product **IV** were found. At pH 12, besides HMETO (which accounted for about 65% of
298 METO degradation) and product **IV**, an additional degradation product was found (product **V**). Like in the
299 case of ACETO, this product, tentatively identified as N-(2-ethyl-6-methylphenyl)-2-methoxy-N-(1-
300 methoxypropan-2-yl)acetamide, might have been formed by methanolysis of METO by nucleophilic
301 substitution of the chlorine atom by CH_3O^- . The formation of both HMETO and product **V** would involve
302 the cleavage of the C–Cl bond as the first rate-limiting step via a $\text{S}_{\text{N}}2$ nucleophilic substitution mechanism,
303 and thus significant and indistinguishable Cl isotope fractionation in METO is expected for both pathways.

304 The morpholinone derivative (product **IV**) might have formed by two different pathways (**Fig. 2**):

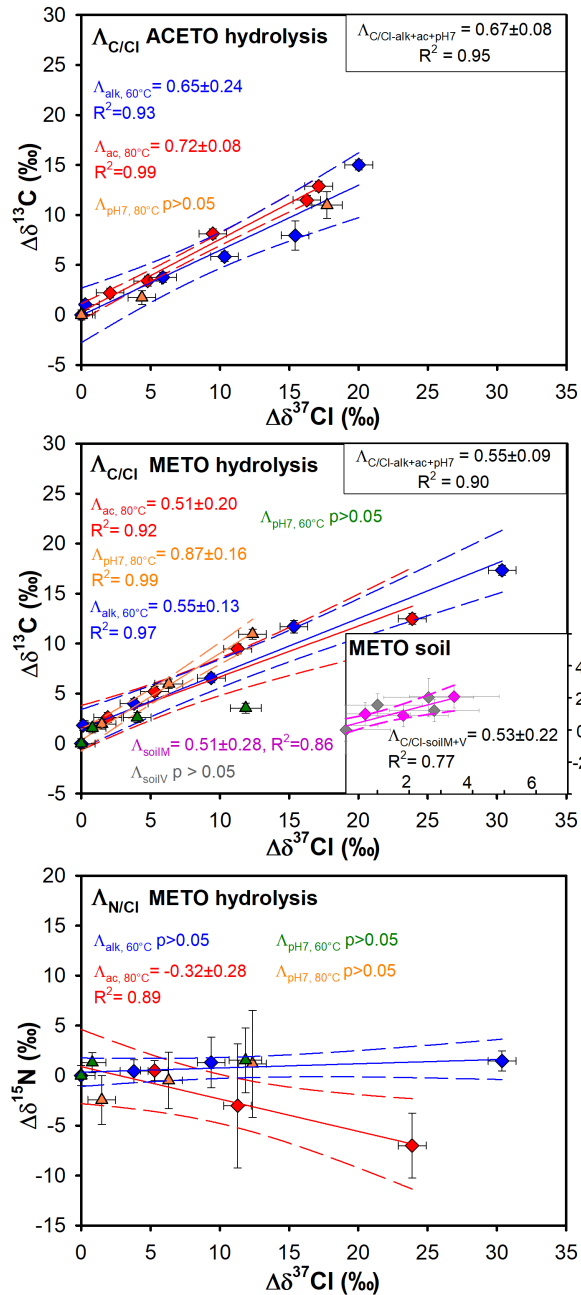
305 (1) $\text{S}_{\text{N}}2$ demethylation at the ether group and subsequent intramolecular $\text{S}_{\text{N}}2$ nucleophilic
306 hydroxide substitution at the C–Cl bond and internal cyclisation²⁷. In this case, the transient
307 appearance of the demethylated product metolachlor-desmethyl (2-Chloro-N-(2-ethyl-6-
308 methylphenyl)-N-(2-hydroxy-1-methylethyl)acetamide) could have been masked by
309 neutralization with NaOH²⁷. Since the first rate-limiting step does not involve the C–Cl bond, Cl
310 isotope fractionation would not be expected for METO degradation through this pathway.

311 (2) Hydrolysis to HMETO and subsequent nucleophilic substitution at the ether C–O bond and ring
312 formation. Here, Cl isotope fractionation would be expected.

313 The reaction time course suggests a co-occurrence of both pathways in equilibrium under all conditions,
314 except for neutral pH at 80°C, where product **IV** seems to be formed only by the pathway involving HMETO
315 as intermediate (**Fig. 2**). The consistent pronounced Cl isotope fractionation ($\epsilon_{\text{Cl}} = -6.5 \pm 0.7\text{‰}$, combining
316 data for all METO hydrolysis experiments), also in comparison to the ACETO data, indicates that the
317 pathways involving C–Cl bond cleavage as the first rate-limiting steps were prominent under all conditions
318 (**Table 1**). According to the prevalence of the hydroxide substitution mechanism, obtained AKIE_{Cl} (from
319 1.006 to 1.012) and AKIE_{C} (from 1.060 to 1.076) values fit in the range of experimentally derived AKIEs
320 from the literature for $\text{S}_{\text{N}}2$ type nucleophilic substitution reactions involving a C–Cl bond^{58, 60, 61} (**Table S9**).

321 Accordingly, insignificant N isotope fractionation was observed under all conditions. Surprisingly, the dual
322 Cl-N approach (**Fig. 3**) shows different patterns for alkaline and acidic hydrolysis of METO, pointing to
323 secondary N inverse isotope effect under acidic conditions. This secondary N isotope effect might be a
324 result of a higher contribution of the O-demethylation pathway at pH 3 and warrants further study.

325 For chloroacetanilides, thus, pronounced carbon and chlorine isotope effects appear to be indicative of
326 both ACETO and METO hydrolysis under a range of different conditions, whereas nitrogen isotope effects
327 are much smaller in magnitude and largely negligible. **Table 1** lists the 2D-slopes ($\Lambda_{N/C}$, $\Lambda_{C/Cl}$ and $\Lambda_{N/Cl}$). A
328 comparison between lambda values and their uncertainties obtained in this study with the OLR and the
329 York⁵⁹ regression methods is shown in the **SI**. There are no statistically significant differences between the
330 dual C-Cl isotope patterns for acidic, alkaline and neutral hydrolysis, including experiments performed at
331 different temperatures. Data from the different experiments were thus merged to derive combined $\Lambda_{C/Cl}$
332 values of 0.67 ± 0.08 for ACETO and 0.55 ± 0.09 for METO hydrolysis (**Fig. 3**). This indicates that C-Cl bond
333 cleavage by an S_N2 reaction is the predominant mechanism under both acidic, alkaline and neutral
334 conditions and that a similar pattern can also be expected in enzymatic reactions. The combined pattern
335 of carbon and chlorine isotope data is thus a promising indicator of natural chloroacetanilide degradation.



336
 337 **Figure 3.** Dual isotope plots for ACETO hydrolysis ($\Delta\delta^{13}C$ vs $\Delta\delta^{37}Cl$), METO hydrolysis ($\Delta\delta^{15}N$ vs $\Delta\delta^{37}Cl$ and
 338 $\Delta\delta^{13}C$ vs $\Delta\delta^{37}Cl$), and METO degradation in soil ($\Delta\delta^{13}C$ vs $\Delta\delta^{37}Cl$). Error bars display the uncertainty
 339 calculated by error propagation. Slopes (Λ values) were calculated by OLR and uncertainty is shown as
 340 95% CI. Displayed linear regression are significant except when noted ($p > 0.05$). When differences
 341 between the regressed data for the different experimental conditions were not significant ($p > 0.05$), data
 342 were merged to derive combined Λ values.

343

344 **Carbon and Chlorine Isotope Fractionation in Chloroacetanilide Biodegradation**

345 METO dissipation in the two soils followed pseudo first order kinetics, with a transformation rate faster
346 in soil V than in soil M (**Fig. S6**). Half-lives ranged between 26 and 86 days (**Table S11**). METO degradation
347 in both soils resulted in the release of ESA and OXA metabolites and traces of HMETO (data not shown),
348 indicating that a thiolytic (glutathione-dependent) dechlorination was the main pathway, in which
349 glutathione S_N2 nucleophilic substitution is the first rate-limiting step.

350 Accordingly, METO degradation in the two soils resulted in primary normal carbon isotope effect. The ϵ_c
351 values obtained in the present experiments (-2.0 ± 1.2 and $-2.6 \pm 1.3\%$) are not significantly different from
352 those reported by Alvarez-Zaldívar et al.⁴², Meite⁴⁴ and Droz et al.⁴⁵ for METO biodegradation in different
353 crop soils and wetland sediments (**Table S12**). Most importantly, our results showed a significant chlorine
354 isotope effect (**Fig. S7**) and thus Cl isotope fractionation appears to be a particularly strong indicator of
355 biodegradation, even more than carbon. Since there are no significant differences between the two soils,
356 data were merged to derive combined ϵ_{Cl} ($-3.3 \pm 1.6\%$) and ϵ_c ($-2.4 \pm 0.8\%$) values. Obtained AKIE_{Cl} (from
357 1.003 to 1.004) and AKIE_C (from 1.031 to 1.040) values (**Table S12**) are also consistent with primary isotope
358 effect during S_N2 type substitution^{58, 60, 61}.

359 METO degradation in the two soils resulted in $\Lambda_{C/Cl}$ values not significantly different and thus a combined
360 $\Lambda_{C/Cl}$ value of 0.53 ± 0.22 was derived (**Fig. 3**). There are no statistically significant differences between the
361 dual C–Cl isotope patterns for METO degradation in soils and by hydrolysis. The isotope trends observed
362 for the METO degradation pathways tested here resulted thus in a robust multi-element isotope
363 fractionation pattern, consistent with C–Cl bond cleavage by an S_N2 nucleophilic substitution in the rate-
364 limiting step for both reactions (hydrolytic and thiolytic glutathione-dependent dechlorination).

365 **Carbon, Chlorine and Nitrogen Isotope Fractionation in ATR abiotic hydrolysis**

366 Based on carbon and nitrogen isotope data alone, it has not been possible so far to clearly distinguish
367 between oxidative N-dealkylation^{22, 63}, which is the main degradation route for ATR, versus alkaline
368 hydrolysis, which is a relevant mechanism on clay surfaces⁵⁴, and oxidation by indirect photolysis⁵⁶. Also,

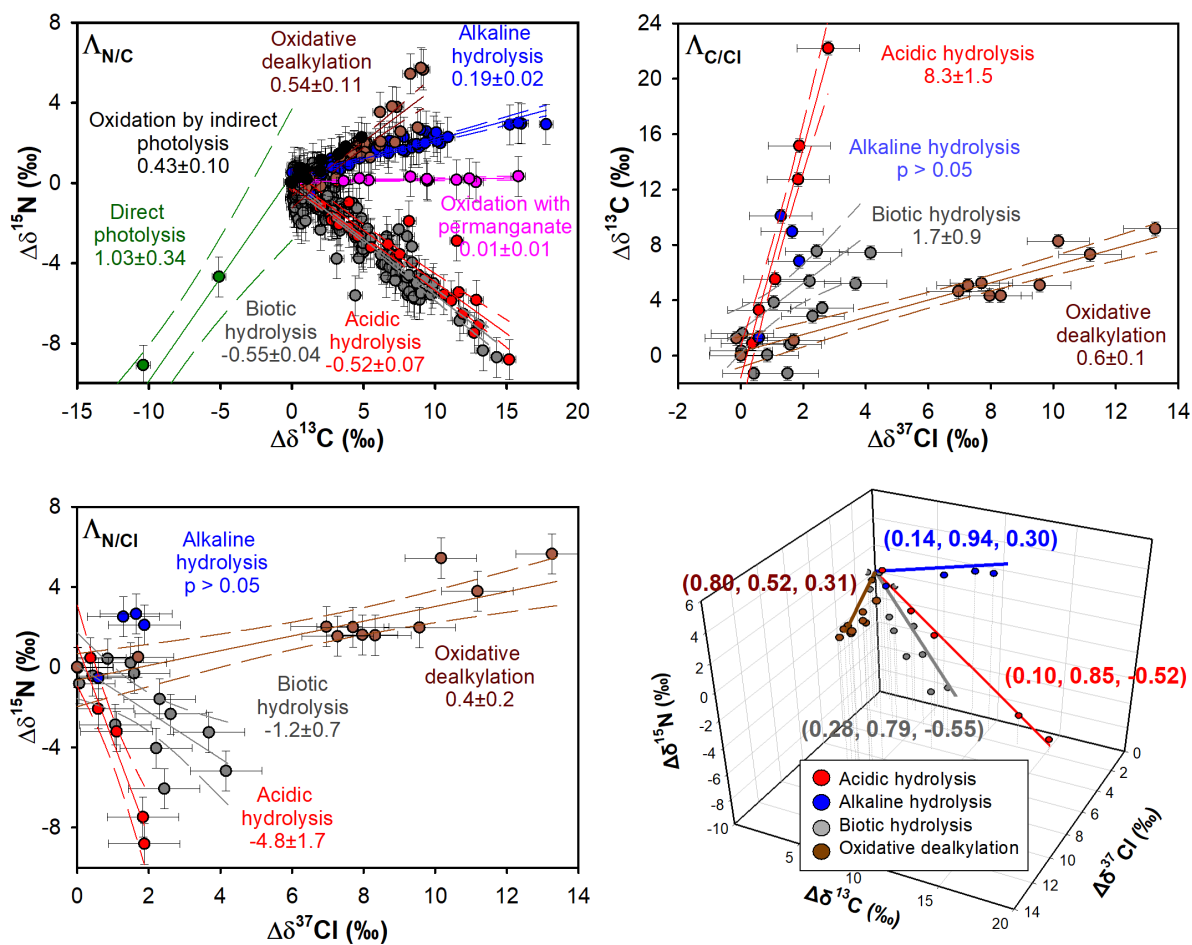
369 $\Lambda_{N/C}$ values do not allow a distinction between acidic hydrolysis and biotic hydrolytic dichlorination^{10, 11, 21-}
370 ^{25, 28} (**Table S14**). One of our goals was, therefore, to investigate whether information gained from Cl
371 isotope fractionation could help in distinguishing between these transformation pathways.

372 Acidic (pH 3, 25°C) and alkaline (pH 12, 25°C) hydrolysis of ATR followed pseudo first order kinetics, with
373 half-lives ranging between 2.6 and 24 days (**Table S13**). In accordance with Masbou et al.²¹, no ATR
374 degradation ($p>0.05$) was observed under neutral conditions (pH 7, 25°C). Also consistent with previous
375 studies^{21, 22, 63, 64}, HATR was produced under both acidic and alkaline conditions (**Fig. S9**), pointing to
376 nucleophilic substitution of the chlorine atom by a hydroxyl group⁶³. The experiments at pH 3 showed a
377 closed mass balance. At pH 12, however, HATR accounted for about 40% of the ATR degradation. An
378 additional degradation product, referred to as product **VI**, was concomitantly formed with HATR. Product
379 **VI** was tentatively identified as 2-Methoxy-4-isopropylamino-6-ethylamino-S-triazine (atraton) (**Fig. S10**).
380 It might have been formed, as occurred for the chloroacetanilides, as a by-product of the hydrolysis
381 experiment in the presence of methanol under alkaline conditions by nucleophilic substitution of the
382 chlorine atom by $\text{CH}_3\text{O}^{-62}$.

383 Characteristic isotope fractionation trends of C and N during acidic and alkaline ATR hydrolysis were
384 observed. At pH 3, the degradation of ATR was accompanied by enrichment in both ³⁷Cl and ¹³C and
385 depletion in ¹⁵N in the remaining substrate (**Fig. S11**). At pH 12, however, hydrolysis of ATR resulted in
386 normal isotope fractionation for the three elements. The chlorine, carbon and nitrogen isotope
387 composition remained constant at pH 7, where no ATR degradation was observed. For both acidic and
388 alkaline hydrolysis, the obtained ϵ_C and ϵ_N values from Rayleigh plots are similar ($p>0.05$) to those reported
389 previously^{21, 22, 63} for temperatures ranging from 20 to 60°C (**Table S14**), confirming that C and N isotope
390 fractionations are not significantly affected by temperature within the uncertainties of ϵ -values²¹. ϵ_{Cl}
391 values are also similar to those previously reported for ATR biodegradation by *Arthrobacter aurescens* TC1
392 ($-1.4\pm 0.6\%$)²⁸, which is expected to occur by an acid-catalyzed hydrolysis²². AKIE_C (1.039 ± 0.003 for acidic
393 and 1.033 ± 0.028 for alkaline hydrolysis) and AKIE_N (0.986 ± 0.002 and 1.0013 ± 0.005 , respectively) values

394 are within the previously reported range for abiotic hydrolysis, and within the range or slightly higher than
395 those reported for microbial hydrolytic dechlorination (AKIE_C from 1.015 to 1.045 and AKIE_N between
396 0.974 and 0.996)^{10, 11, 22-26, 28}. AKIE_C values for both acidic and alkaline hydrolysis are consistent with a
397 primary isotope effect during an $\text{S}_{\text{N}}2$ type mechanism ($\text{AKIE}_C = 1.03 - 1.09$)⁵⁸. AKIE_{Cl} (1.0005 ± 0.0001 for
398 acidic and 1.0006 ± 0.0002 for alkaline hydrolysis) values are much smaller than the semiclassical
399 Streitwieser limit for KIE_{Cl} in C-Cl bonds (1.013)⁵⁸ and that the typical range for $\text{S}_{\text{N}}2$ reactions^{60, 61},
400 suggesting that the C-Cl bond is not cleaved in the rate-determining step and the chlorine isotope effect
401 is masked, as observed in our previous study²⁸.

402 Dual isotope plots (C-N, C-Cl and N-Cl) for different ATR transformation reactions are shown in **Figure 4**.
403 These dual isotope plots are based on our data and on data from previous studies on acidic^{21, 22}, alkaline^{21,}
404 ^{22, 63}, and biotic hydrolysis^{11, 22-25, 28} as well as oxidative dealkylation^{28, 55}, oxidation by indirect photolysis
405 by 4-carboxybenzophenone or OH radical⁵⁶, direct photolysis⁵⁶, and oxidation with permanganate⁵⁵.
406 Statistical comparisons of the corresponding regression data are shown in **Table S15**, which lists results
407 of the z-score tests for all possible pairings of dual isotope slopes. From the combination of C and Cl
408 isotope data, acidic hydrolysis and microbial hydrolytic dechlorination can now be distinguished, which
409 was not the case with C and N data only. With this dual C-Cl isotope plot, one could potentially distinguish
410 microbial oxidative dealkylation from the three hydrolytic reactions. Although further research is required
411 for a determination of $\Lambda_{\text{N-Cl}}$ for alkaline hydrolysis, the N-Cl correlations are promising for distinguishing
412 the four reactions, given that all $\Lambda_{\text{N/Cl}}$ values are significantly different from each other.



413

414 **Figure 4.** Dual isotope plots and corresponding slopes ($\Lambda_{N/C}$, $\Lambda_{C/Cl}$, $\Lambda_{N/Cl}$), and multi-element (C, N and Cl)

415 isotope fractionation patterns for different ATR degradation processes. Slopes for dual isotope plots were

416 calculated by OLR of data from our experiments and data extracted from previous studies. Uncertainty is

417 shown as 95% CI. The following transformation processes were assessed: abiotic alkaline hydrolysis (this

418 study)^{21, 22, 63}, abiotic acidic hydrolysis (this study)^{21, 22}, oxidative dealkylation by *Rhodococcus* sp.

419 NI86/21^{28, 55}, oxidation with permanganate⁵⁵, oxidation by indirect photolysis by 4-carboxybenzophenone

420 or OH· radicals⁵⁶, direct photolysis⁵⁶, and enzymatic hydrolysis by different strains (*Arthrobacter aurescens*

421 TC1, *Chelatobacter heintzii*, *Pseudomonas* sp. ADP, *Ensifer* sp. CX-T, *Sinorhizobium* sp. K, *Polaromonas* sp.

422 Nea-C and *Rhizobium* sp. CX-Z)^{10, 11, 22-25, 28}. Error bars display uncertainties of $\pm 0.5\text{‰}$ for C and $\pm 1.0\text{‰}$ for

423 Cl and N. The 3D plot shows isotope fractionation patterns during degradation of ATR by abiotic acidic

424 hydrolysis (red), abiotic alkaline hydrolysis (blue), biotic hydrolysis by *Arthrobacter aurescens* TC1 (grey)²⁸

425 and oxidative dealkylation by *Rhodococcus* sp. NI86/21 (brown)²⁸. Each isotope fractionation trend was

426 characterized by principal component analysis in SigmaPlot v.14.0⁶⁵. Characteristic unit vectors (indicated

427 in brackets) were determined for each degradation pathway. The corresponding eigenvectors and

428 standard errors are shown in **Table S16**.

429 C, N and Cl isotope data for ATR abiotic hydrolysis from this study and biodegradation²⁸ were also
430 combined in a 3D isotope plot. Characteristic unit vectors were determined for each degradation pathway
431 following the approach of Palau et al.⁶⁵ (**Fig. 4**). This plot shows clearly different trends for the four
432 degradation pathways, allowing now a clear distinction between oxidative dealkylation and alkaline
433 hydrolysis, which was difficult based on C and N data only. The angles between the obtained unit vectors
434 are shown in **Table S17**.

435 **Environmental significance**

436 By bringing forward the first dataset on chlorine isotope fractionation in chloroacetanilide degradation,
437 and new data in atrazine degradation, our study highlights the benefit of including Cl isotope analysis into
438 future transformation studies of pesticides. For a reliable mechanistic interpretation of pesticide isotopic
439 fractionation in field studies, reference multi-isotopic fractionation values need to be obtained from
440 model, environmentally relevant transformation reactions, such as abiotic hydrolysis, as it can also be
441 mediated by microorganisms.

442 For ACETO and METO, Cl isotope will be a sensitive indicator of transformation reactions for future lab
443 and field applications, even if the extent of degradation is limited. Indeed, applying the determined ϵ
444 values, with a chloroacetanilides degradation extent of only 25-30%, a detectable positive shift in chlorine
445 isotope values of 2‰ would occur. The reactions tested here, where bimolecular substitution occurs at
446 the C-Cl bond in the rate-determining step, provide a robust multi-element isotope fractionation pattern
447 that will be easily recognizable in the field. Further laboratory data need to be produced to constrain the
448 multi-element isotope fractionation ranges for other chloroacetanilide transformation pathways such as
449 microbial N-dealkylation, microbial degradation under anaerobic conditions or photodegradation.

450 The benefit of including Cl isotope analysis is clearly shown also for ATR, for which the 3D-CSIA approach
451 allowed closing research gaps by differentiating degradation pathways that were not possible to
452 distinguish based on previous studies without Cl isotope data (*e.g.*, oxidative dealkylation and alkaline
453 hydrolysis; acidic hydrolysis and biotic hydrolysis). The clearly distinct isotope patterns for the different

454 ATR degradation pathways open the possibility of a multi-element (Cl, C, N) isotope approach to identify
455 these different pathways in the field.

456 Therefore, the 3D-CSIA approach we used for characterizing abiotic hydrolysis of ACETO, METO and ATR,
457 as well as METO biodegradation in two soils, provides the basis for studying the fate and distinguishing
458 degradation processes of these herbicides in the field. Understanding what mechanism lies behind the
459 isotope effects observed in the field would allow choosing an appropriate ϵ value for quantification of
460 natural or enhanced pesticide attenuation. Some analytical challenges associated to the application of
461 CSIA to pesticides, mainly related to their low (sub- $\mu\text{g/L}$) environmental concentrations, high molecular
462 size, and high polarity, have recently been overcome^{9, 30}, which will allow further application of multi-
463 element CSIA in environmental samples.

464 **AUTHOR INFORMATION**

465 **Corresponding Author**

466 *Phone: +34 93 403 37 73; e-mail: clara.torrento@gmail.com

467 **Present Addresses**

468 †Present Address: Grup MAiMA, Departament de Mineralogia, Petrologia i Geologia Aplicada, Facultat de
469 Ciències de la Terra, Universitat de Barcelona (UB), C/ Martí i Franquès s/n, 08028, Barcelona, Spain.

470 ‡Present Address: Département des sciences de la Terre et de l'atmosphère, Université du Québec à
471 Montréal, 201 avenue du Président Kennedy, Montréal, QC, Canada.

472 **ACKNOWLEDGMENTS**

473 This study was supported by the project CRSII2_141805/1 from the Swiss National Science Foundation
474 (SNSF). Soil experiments were supported by BRGM funding (DEV REPERER project). The authors would
475 like to thank Jakov Bolotin (Eawag), Gaétan Glauser (Neuchâtel Platform of Analytical Chemistry) and
476 Benjamin Girardeau (BRGM) for their help in the laboratory.

477 **SUPPORTING INFORMATION**

478 Chemicals and additional details for the experiments, analytical methods, determination of AKIEs, spiked
479 tests for soils experiments, degradation kinetics, degradation products and obtained isotope data for
480 chloroacetanilides abiotic hydrolysis, metolachlor degradation in soil and atrazine abiotic hydrolysis.

481 REFERENCES

- 482 1. FAO FAOSTAT Pesticides Use Dataset. Available at <http://www.fao.org/faostat/en/#data/RP>.
483 Accessed June 2021. Rome, Food and Agriculture Organization of the United Nations (FAO).
- 484 2. Kim, K.-H.; Kabir, E.; Jahan, S. A., Exposure to pesticides and the associated human health effects.
485 *Sci Total Environ* **2017**, *575*, 525-535.
- 486 3. Vijver, M. G.; Hunting, E. R.; Nederstigt, T. A. P.; Tamis, W. L. M.; Van Den Brink, P. J.; Van
487 Bodegom, P. M., Postregistration monitoring of pesticides is urgently required to protect ecosystems.
488 *Environ. Toxicol. Chem.* **2017**, *36*, (4), 860-865.
- 489 4. Fenner, K.; Canonica, S.; Wackett, L. P.; Elsner, M., Evaluating Pesticide Degradation in the
490 Environment: Blind Spots and Emerging Opportunities. *Science* **2013**, *341*, (6147), 752.
- 491 5. Fenner, K.; Elsner, M.; Lueders, T.; McLachlan, M. S.; Wackett, L. P.; Zimmermann, M.; Drewes, J.
492 E., Methodological Advances to Study Contaminant Biotransformation: New Prospects for Understanding
493 and Reducing Environmental Persistence? *ACS ES&T Water* **2021**, *1*, (7), 1541-1554.
- 494 6. Farlin, J.; Bayerle, M.; Pittois, D.; Gallé, T., Estimating Pesticide Attenuation From Water Dating
495 and the Ratio of Metabolite to Parent Compound. *Groundwater* **2017**, *55*, (4), 550-557.
- 496 7. Elsner, M.; Imfeld, G., Compound-specific isotope analysis (CSIA) of micropollutants in the
497 environment — current developments and future challenges. *Curr. Opin. Biotechnol.* **2016**, *41*, 60-72.
- 498 8. Torrentó, C.; Bakkour, R.; Glauser, G.; Melsbach, A.; Ponsin, V.; Hofstetter, T. B.; Elsner, M.;
499 Hunkeler, D., Solid-phase extraction method for stable isotope analysis of pesticides from large volume
500 environmental water samples. *Analyst* **2019**, *144*, (9), 2898-2908.
- 501 9. Melsbach, A.; Ponsin, V.; Torrento, C.; Lihl, C.; Hofstetter, T. B.; Hunkeler, D.; Elsner, M., (13)C-
502 and (15)N-Isotope Analysis of Desphenylchloridazon by Liquid Chromatography-Isotope-Ratio Mass
503 Spectrometry and Derivatization Gas Chromatography-Isotope-Ratio Mass Spectrometry. *Anal. Chem.*
504 **2019**, *91*, (5), 3412-3420.
- 505 10. Ehrl, B. N.; Kundu, K.; Gharasoo, M.; Marozava, S.; Elsner, M., Rate-Limiting Mass Transfer in
506 Micropollutant Degradation Revealed by Isotope Fractionation in Chemostat. *Environ. Sci. Technol.* **2019**,
507 *53*, (3), 1197-1205.
- 508 11. Ehrl, B. N.; Gharasoo, M.; Elsner, M., Isotope Fractionation Pinpoints Membrane Permeability as
509 a Barrier to Atrazine Biodegradation in Gram-negative Polaromonas sp. Nea-C. *Environ. Sci. Technol.* **2018**,
510 *52*, (7), 4137-4144.
- 511 12. Ojeda, A. S.; Phillips, E.; Sherwood Lollar, B., Multi-element (C, H, Cl, Br) stable isotope
512 fractionation as a tool to investigate transformation processes for halogenated hydrocarbons. *Environ.*
513 *Sci. Process. Impact* **2020**, *22*, 567-582.
- 514 13. Nijenhuis, I.; Renpenning, J.; Kümmel, S.; Richnow, H. H.; Gehre, M., Recent advances in multi-
515 element compound-specific stable isotope analysis of organohalides: Achievements, challenges and
516 prospects for assessing environmental sources and transformation. *Trends Environ. Anal. Chem.* **2016**, *11*,
517 1-8.
- 518 14. Vogt, C.; Dorer, C.; Musat, F.; Richnow, H.-H., Multi-element isotope fractionation concepts to
519 characterize the biodegradation of hydrocarbons — from enzymes to the environment. *Curr. Opin.*
520 *Biotechnol.* **2016**, *41*, 90-98.
- 521 15. Elsner, M., Stable isotope fractionation to investigate natural transformation mechanisms of
522 organic contaminants: Principles, prospects and limitations. *Journal of Environmental Monitoring* **2010**,
523 *12*, (11), 2005-2031.

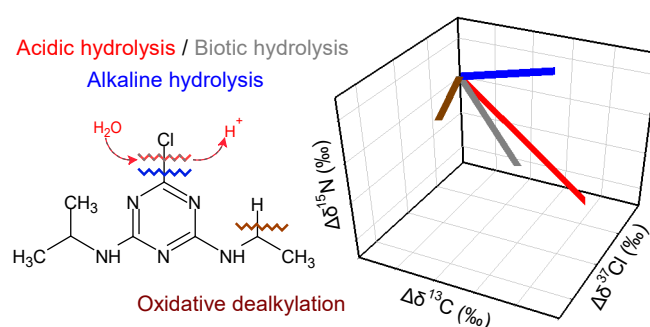
- 524 16. Penning, H.; Cramer, C. J.; Elsner, M., Rate-Dependent Carbon and Nitrogen Kinetic Isotope
525 Fractionation in Hydrolysis of Isoproturon. *Environ. Sci. Technol.* **2008**, *42*, (21), 7764-7771.
- 526 17. Penning, H.; Elsner, M., Intramolecular Carbon and Nitrogen Isotope Analysis by Quantitative Dry
527 Fragmentation of the Phenylurea Herbicide Isoproturon in a Combined Injector/Capillary Reactor Prior to
528 GC Separation. *Anal. Chem.* **2007**, *79*, (21), 8399-8405.
- 529 18. Penning, H.; Sørensen, S. R.; Meyer, A. H.; Aamand, J.; Elsner, M., C, N, and H Isotope Fractionation
530 of the Herbicide Isoproturon Reflects Different Microbial Transformation Pathways. *Environ. Sci. Technol.*
531 **2010**, *44*, (7), 2372-2378.
- 532 19. Wu, L.; Chládková, B.; Lechtenfeld, O. J.; Lian, S.; Schindelka, J.; Herrmann, H.; Richnow, H. H.,
533 Characterizing chemical transformation of organophosphorus compounds by ¹³C and ²H stable isotope
534 analysis. *Sci Total Environ* **2018**, *615*, 20-28.
- 535 20. Wu, L.; Kümmel, S.; Richnow, H. H., Validation of GC-IRMS techniques for $\delta^{13}\text{C}$ and $\delta^2\text{H}$ CSIA of
536 organophosphorus compounds and their potential for studying the mode of hydrolysis in the
537 environment. *Anal. Bioanal. Chem.* **2017**, *409*, (10), 2581-2590.
- 538 21. Masbou, J.; Drouin, G.; Payraudeau, S.; Imfeld, G., Carbon and nitrogen stable isotope
539 fractionation during abiotic hydrolysis of pesticides. *Chemosphere* **2018**, *213*, 368-376.
- 540 22. Meyer, A. H.; Penning, H.; Elsner, M., C and N Isotope Fractionation Suggests Similar Mechanisms
541 of Microbial Atrazine Transformation Despite Involvement of Different Enzymes (AtzA and TrzN). *Environ.*
542 *Sci. Technol.* **2009**, *43*, (21), 8079-8085.
- 543 23. Schürner, H. K. V.; Seffernick, J. L.; Grzybkowska, A.; Dybala-Defratyka, A.; Wackett, L. P.; Elsner,
544 M., Characteristic Isotope Fractionation Patterns in s-Triazine Degradation Have Their Origin in Multiple
545 Protonation Options in the s-Triazine Hydrolase TrzN. *Environ. Sci. Technol.* **2015**, *49*, (6), 3490-3498.
- 546 24. Chen, S.; Yang, P.; Rohit kumar, J.; Liu, Y.; Ma, L., Inconsistent carbon and nitrogen isotope
547 fractionation in the biotransformation of atrazine by *Ensifer* sp. CX-T and *Sinorhizobium* sp. K. *Int.*
548 *Biodeter. Biodeg.* **2017**, *125*, 170-176.
- 549 25. Chen, S.; Zhang, K.; Jha, R. K.; Chen, C.; Yu, H.; Liu, Y.; Ma, L., Isotope fractionation in atrazine
550 degradation reveals rate-limiting, energy-dependent transport across the cell membrane of gram-
551 negative rhizobium sp. CX-Z. *Environ. Pollut.* **2019**, *248*, 857-864.
- 552 26. Chen, S.; Zhang, K.; Jha, R. K.; Ma, L., Impact of atrazine concentration on bioavailability and
553 apparent isotope fractionation in Gram-negative Rhizobium sp. CX-Z. *Environ. Pollut.* **2019**, *257*, 113614.
- 554 27. Carlson, D. L.; Than, K. D.; Roberts, A. L., Acid- and Base-Catalyzed Hydrolysis of Chloroacetamide
555 Herbicides. *J. Agric. Food. Chem.* **2006**, *54*, (13), 4740-4750.
- 556 28. Lihl, C.; Heckel, B.; Grzybkowska, A.; Dybala-Defratyka, A.; Ponsin, V.; Torrentó, C.; Hunkeler, D.;
557 Elsner, M., Compound-Specific Chlorine Isotope Fractionation in Biodegradation of Atrazine. *Environ. Sci.*
558 *Process. Impact* **2020**, *22*, 792-801.
- 559 29. Li, S.; Elliott, D. W.; Spear, S. T.; Ma, L.; Zhang, W.-X., Hexachlorocyclohexanes in the Environment:
560 Mechanisms of Dechlorination. *Critical Reviews in Environmental Science and Technology* **2011**, *41*, (19),
561 1747-1792.
- 562 30. Ponsin, V.; Torrentó, C.; Lihl, C.; Elsner, M.; Hunkeler, D., Compound-specific chlorine isotope
563 analysis of the herbicides atrazine, acetochlor and metolachlor. *Anal. Chem.* **2019**, *91*, (22), 14290-14298.
- 564 31. Imfeld, G.; Besaury, L.; Maucourt, B.; Donadello, S.; Baran, N.; Vuilleumier, S., Toward Integrative
565 Bacterial Monitoring of Metolachlor Toxicity in Groundwater. *Front. Microbiol.* **2018**, *9*, (2053).
- 566 32. Hladik, M. L.; Bouwer, E. J.; Roberts, A. L., Neutral chloroacetamide herbicide degradates and
567 related compounds in Midwestern United States drinking water sources. *Sci Total Environ* **2008**, *390*, (1),
568 155-165.
- 569 33. Amalric, L.; Baran, N.; Coureau, C.; Maingot, L.; Buron, F.; Routier, S., Analytical developments for
570 47 pesticides: first identification of neutral chloroacetanilide derivatives in French groundwater.
571 *International Journal of Environmental Analytical Chemistry* **2013**, *93*, (15), 1660-1675.
- 572 34. Baran, N.; Gourcy, L., Sorption and mineralization of S-metolachlor and its ionic metabolites in
573 soils and vadose zone solids: Consequences on groundwater quality in an alluvial aquifer (Ain Plain,
574 France). *J. Contam. Hydrol.* **2013**, *154*, 20-28.

- 575 35. Reemtsma, T.; Alder, L.; Banasiak, U., Emerging pesticide metabolites in groundwater and surface
576 water as determined by the application of a multimethod for 150 pesticide metabolites. *Water Res.* **2013**,
577 *47*, (15), 5535-5545.
- 578 36. Field, J. A.; Thurman, E. M., Glutathione Conjugation and Contaminant Transformation. *Environ.*
579 *Sci. Technol.* **1996**, *30*, (5), 1413-1418.
- 580 37. Graham, W. H.; Graham, D. W.; deNoyelles, F.; Smith, V. H.; Larive, C. K.; Thurman, E. M.,
581 Metolachlor and Alachlor Breakdown Product Formation Patterns in Aquatic Field Mesocosms. *Environ.*
582 *Sci. Technol.* **1999**, *33*, (24), 4471-4476.
- 583 38. Loch, A. R.; Lippa, K. A.; Carlson, D. L.; Chin, Y. P.; Traina, S. J.; Roberts, A. L., Nucleophilic Aliphatic
584 Substitution Reactions of Propachlor, Alachlor, and Metolachlor with Bisulfide (HS-) and Polysulfides (Sn₂-
585). *Environ. Sci. Technol.* **2002**, *36*, (19), 4065-4073.
- 586 39. Gan, J.; Wang, Q.; Yates, S. R.; Koskinen, W. C.; Jury, W. A., Dechlorination of chloroacetanilide
587 herbicides by thiosulfate salts. *PNAS* **2002**, *99*, (8), 5189-5194.
- 588 40. Cai, X.; Sheng, G.; Liu, W., Degradation and detoxification of acetochlor in soils treated by organic
589 and thiosulfate amendments. *Chemosphere* **2007**, *66*, (2), 286-292.
- 590 41. Maillard, E.; Lange, J.; Schreiber, S.; Dollinger, J.; Herbstritt, B.; Millet, M.; Imfeld, G., Dissipation
591 of hydrological tracers and the herbicide S-metolachlor in batch and continuous-flow wetlands.
592 *Chemosphere* **2016**, *144*, 2489-2496.
- 593 42. Alvarez-Zaldívar, P.; Payraudeau, S.; Meite, F.; Masbou, J.; Imfeld, G., Pesticide degradation and
594 export losses at the catchment scale: Insights from compound-specific isotope analysis (CSIA). *Water Res.*
595 **2018**, *139*, 198-207.
- 596 43. Torabi, E.; Wiegert, C.; Guyot, B.; Vuilleumier, S.; Imfeld, G., Dissipation of S-metolachlor and
597 butachlor in agricultural soils and responses of bacterial communities: Insights from compound-specific
598 isotope and biomolecular analyses. *Journal of Environmental Sciences* **2020**, *92*, 163-175.
- 599 44. Meite, F. Transformation and transport of inorganic and synthetic pesticides in soils of agricultural
600 catchments. PhD Thesis. University of Strasbourg, 407 p., 2018.
- 601 45. Droz, B.; Drouin, G.; Maurer, L.; Villette, C.; Payraudeau, S.; Imfeld, G., Phase Transfer and
602 Biodegradation of Pesticides in Water–Sediment Systems Explored by Compound-Specific Isotope
603 Analysis and Conceptual Modeling. *Environ. Sci. Technol.* **2021**, *55*, (8), 4720-4728.
- 604 46. Sanyal, D.; Yaduraju, N. T.; Kulshrestha, G., Metolachlor persistence in laboratory and field soils
605 under Indian tropical conditions. *J Environ Sci Health B* **2000**, *35*, (5), 571-583.
- 606 47. White, P. M.; Potter, T. L.; Bosch, D. D.; Joo, H.; Schaffer, B.; Muñoz-Carpena, R., Reduction in
607 Metolachlor and Degradate Concentrations in Shallow Groundwater through Cover Crop Use. *J. Agric.*
608 *Food. Chem.* **2009**, *57*, (20), 9658-9667.
- 609 48. Hladik, M. L.; Hsiao, J. J.; Roberts, A. L., Are Neutral Chloroacetamide Herbicide Degradates of
610 Potential Environmental Concern? Analysis and Occurrence in the Upper Chesapeake Bay. *Environ. Sci.*
611 *Technol.* **2005**, *39*, (17), 6561-6574.
- 612 49. Elsayed, O. F.; Maillard, E.; Vuilleumier, S.; Nijenhuis, I.; Richnow, H. H.; Imfeld, G., Using
613 compound-specific isotope analysis to assess the degradation of chloroacetanilide herbicides in lab-scale
614 wetlands. *Chemosphere* **2014**, *99*, 89-95.
- 615 50. Cessna, A. J., Nonbiological Degradation of Triazine Herbicides: Photolysis and Hydrolysis. In *The*
616 *triazine herbicides: 50 years Revolutionizing Agriculture*, Lebaron, H.; McFarland, J. E.; Burnside, O. C., Eds.
617 Elsevier: Amsterdam, The Netherlands, 2008; pp. 329-353. In.
- 618 51. Wackett, L.; Sadowsky, M.; Martinez, B.; Shapir, N., Biodegradation of atrazine and related s-
619 triazine compounds: from enzymes to field studies. *Appl. Microbiol. Biotechnol.* **2002**, *58*, (1), 39-45.
- 620 52. Govantes, F.; Porrúa, O.; García-González, V.; Santero, E., Atrazine biodegradation in the lab and
621 in the field: enzymatic activities and gene regulation. *Microb. Biotechnol.* **2009**, *2*, (2), 178-185.
- 622 53. Udiković-Kolić, N.; Scott, C.; Martin-Laurent, F., Evolution of atrazine-degrading capabilities in the
623 environment. *Appl. Microbiol. Biotechnol.* **2012**, *96*, (5), 1175-1189.
- 624 54. Xu, J. C.; Stucki, J. W.; Wu, J.; Kostka, J. E.; Sims, G. K., Fate of atrazine and alachlor in redox-treated
625 ferruginous smectite. *Environ. Toxicol. Chem.* **2001**, *20*, (12), 2717-2724.

- 626 55. Meyer, A. H.; Dybala-Defratyka, A.; Alaimo, P. J.; Geronimo, I.; Sanchez, A. D.; Cramer, C. J.; Elsner,
 627 M., Cytochrome P450-catalyzed dealkylation of atrazine by *Rhodococcus* sp. strain NI86/21 involves
 628 hydrogen atom transfer rather than single electron transfer. *Dalton Trans.* **2014**, *43*, (32), 12175-12186.
- 629 56. Hartenbach, A. E.; Hofstetter, T. B.; Tentscher, P. R.; Canonica, S.; Berg, M.; Schwarzenbach, R. P.,
 630 Carbon, Hydrogen, and Nitrogen Isotope Fractionation During Light-Induced Transformations of Atrazine.
 631 *Environ. Sci. Technol.* **2008**, *42*, (21), 7751-7756.
- 632 57. Plust, S. J.; Loehe, J. R.; Feher, F. J.; Benedict, J. H.; Herbrandson, H. F., Kinetics and mechanism of
 633 hydrolysis of chloro-1,3,5-triazines. Atrazine. *J. Org. Chem.* **1981**, *46*, (18), 3661-3665.
- 634 58. Elsner, M.; Zwank, L.; Hunkeler, D.; Schwarzenbach, R. P., A New Concept Linking Observable
 635 Stable Isotope Fractionation to Transformation Pathways of Organic Pollutants. *Environ. Sci. Technol.*
 636 **2005**, *39*, (18), 6896-6916.
- 637 59. Ojeda, A. S.; Phillips, E.; Mancini, S. A.; Lollar, B. S., Sources of Uncertainty in Biotransformation
 638 Mechanistic Interpretations and Remediation Studies using CSIA. *Anal. Chem.* **2019**, *91*, (14), 9147-9153.
- 639 60. Dybala-Defratyka, A.; Rostkowski, M.; Matsson, O.; Westaway, K. C.; Paneth, P., A New
 640 Interpretation of Chlorine Leaving Group Kinetic Isotope Effects; A Theoretical Approach. *J. Org. Chem.*
 641 **2004**, *69*, (15), 4900-4905.
- 642 61. Sicinska, D.; Rostkowski, M.; Paneth, P., Chlorine Isotope Effects on Chemical Reactions. *Current*
 643 *Organic Chemistry* **2005**, *9*, (1), 75-88.
- 644 62. Phan, T. B.; Mayr, H., Comparison of the nucleophilicities of alcohols and alkoxides. *Canadian*
 645 *Journal of Chemistry* **2005**, *83*, (9), 1554-1560.
- 646 63. Meyer, A. H.; Penning, H.; Lowag, H.; Elsner, M., Precise and Accurate Compound Specific Carbon
 647 and Nitrogen Isotope Analysis of Atrazine: Critical Role of Combustion Oven Conditions. *Environ. Sci.*
 648 *Technol.* **2008**, *42*, (21), 7757-7763.
- 649 64. Prosen, H.; Zupančič-Kralj, L., Evaluation of photolysis and hydrolysis of atrazine and its first
 650 degradation products in the presence of humic acids. *Environ. Pollut.* **2005**, *133*, (3), 517-529.
- 651 65. Palau, J.; Shouakar-Stash, O.; Hatijah Mortan, S.; Yu, R.; Rosell, M.; Marco-Urrea, E.; Freedman, D.
 652 L.; Aravena, R.; Soler, A.; Hunkeler, D., Hydrogen Isotope Fractionation during the Biodegradation of 1,2-
 653 Dichloroethane: Potential for Pathway Identification Using a Multi-element (C, Cl, and H) Isotope
 654 Approach. *Environ. Sci. Technol.* **2017**, *51*, (18), 10526-10535.

655

656 **Graphic for Table of Contents (TOC)**



657